Seismic evidence of gas hydrate and seafloor fluid escape on the upper Amazon deep-sea fan, Brazilian equatorial margin

Daniel Praeg, Cleverson Guizan Silva, A. Tadeu Dos Reis, Alberto Cruz, João Marcelo Ketzer, Sébastien Migeon, Christian Gorini

▶ **To cite this version:**

Daniel Praeg, Cleverson Guizan Silva, A. Tadeu Dos Reis, Alberto Cruz, João Marcelo Ketzer, et al.. Seismic evidence of gas hydrate and seafloor fluid escape on the upper Amazon deep-sea fan, Brazilian equatorial margin. Brazilian Journal of Geophysics, 2022, 40 (3), 10.22564/brjg.v40i3.2175 . hal-03984456

HAL Id: hal-03984456
https://hal.science/hal-03984456v1

Submitted on 12 Feb 2023

HAL is a multi-disciplinary open access archive for the deposit and dissemination of scientific research documents, whether they are published or not. The documents may come from teaching and research institutions in France or abroad, or from public or private research centers.

L'archive ouverte pluridisciplinaire **HAL**, est destinée au dépôt et à la diffusion de documents scientifiques de niveau recherche, publiés ou non, émanant des établissements d'enseignement et de recherche français ou étrangers, des laboratoires publics ou privés.

Public Domain

Brazilian Journal of Geophysics (2022) 40, 3, 1-23
© 2022 Brazilian Geophysical Society
ISSN 2764-8044
DOI: 10.22564/brjg.v40i3.2175

SEISMIC EVIDENCE OF GAS HYDRATE AND SEAFLOOR FLUID ESCAPE ON THE UPPER AMAZON DEEP-SEA FAN, BRAZILIAN EQUATORIAL MARGIN

Daniel Praeg [1,2], Cleverson Guizan Silva [3], A. Tadeu dos Reis [4], Alberto Cruz [5], João Marcelo Ketzer [6], Sébastien Migeon [2], Christian Gorini[1]

[1]Sorbonne Université, Institut des Sciences de la Terre de Paris (ISTeP), 4 place Jussieu, 75252 Paris, France – E-mail: praeg@geoazur.unice.fr, christian.gorini@gmail.com

[2]Géoazur, Campus Azur de CNRS, 250 rue Albert Einstein, CS 10269, 06905 Sophia Antipolis, France – E-mail: migeon@geoazur.unice.fr

[3]Universidade Federal Fluminense (UFF), Departamento de Geologia e Geofísica, Av. Gen. Milton Tavares de Souza s.n., Niterói RJ, Brazil – E-mail: cguizan@id.uff.br

[4]Universidade do Estado do Rio de Janeiro (UERJ), Faculdade de Oceanografia, Rua São Franscisco Xavier 524, Maracanã, 20.550-900 Rio de Janeiro, RJ, Brazil – E-mail: tadeu.reis@gmail.com

[5]Beicip-Franlab, Avenida Presidente Wilson 231, Rio de Janeiro, RJ, Brazil – E-mail: albertomcruz88@gmail.com

[6]Linnéuniversitetet, Department of Biology and Environmental Science, 391 82 Kalmar, Sweden – E-mail: marcelo.ketzer@lnu.se

ABSTRACT. The Amazon fan contains a gas hydrate province known from a bottom-simulating reflection (BSR) that lies within an upper slope compressional belt. In this study, the extent and character of the BSR and its relation to thrust-fold structures is examined using a grid of 2D and 3D seismic data. We show the BSR to comprise a series of elongate patches up to 16 km wide that are present along 300 km of the slope in water depths of 750-2250 m and extend over a total area of 6800 km^2. The elongate BSR patches show a strong spatial correspondence with the arcuate crests of thrust-fold anticlines. In profile, the BSR patches exhibit convex forms and/or locally irregular relief that rises toward the seafloor. In plan, 3D seismic horizon maps reveal columnar BSR elevations up to 1 km wide, which rise beneath seafloor mounds and depressions, up to 0.5 km wide and 30 m in relief, interpreted as small mud volcanoes and possible pockmarks. The elongate BSR patches are interpreted to record the structurally-controlled rise of warm, gas-rich fluids into the crests of thrust-folds and their leakage into the gas hydrate stability zone, and in places to seafloor, through a near-surface system of faults, hydrofractures and vents.

Keywords: marine 2D/3D seismic; bottom-simulating reflection; thrust-fold anticlines; gas hydrates; fluid vents

INTRODUCTION

Gas hydrates are ice-like compounds of water and gas molecules that are stable in the relatively high pressures and low temperatures of deep-marine settings, and are commonly encountered within continental slope sediments where there are thermogenic or microbial sources of natural gas (Sloan 2003). An understanding of the extent of frozen deposits of gas hydrate on continental margins has broad implications for global carbon budgets (Archer et al. 2009), for regional geohazards (Maslin et al. 2010), and for assessments of unconventional resources (Boswell and Collett 2011). The most common indicator of the presence of submarine gas hydrate is a bottom-simulating reflection (BSR), inferred to correspond to the phase boundary separating an upper interval in which gas hydrate is stable from a lower interval containing free gas (Shipley et al. 1979; Hillman et al. 2017). Comparisons to drilling data indicate that BSRs primarily result from the impedance contrast due to even small amounts (1%) of free gas, and are poorly correlated to presence of gas hydrate bearing intervals, which moreover may be present in the absence of a BSR (Holbrook et al. 1996; Majumdar et al. 2016). BSRs are typically discontinuous or 'patchy' over a range of scales, to a degree that depends in part on the characteristics of the seismic data used, but also reflects variations in the properties of the host formation and the saturations of gas and gas hydrate (Shedd et al. 2012). At basin scale, a BSR is understood to be a useful minimum indicator of the distribution of gas hydrate (Hillman et al. 2017), the full extent of which remains to be determined.

Gas hydrate provinces have been identified from BSRs in two main areas of the Brazilian continental margin, on the Rio Grande cone of the Pelotas Basin in the south and on the Amazon fan of the Foz do Amazonas Basin in the equatorial region (Manley and Flood 1988; Fontana and Mussumeci 1994; Sad et al. 1998). Whereas the Rio Grande cone is characterised by a BSR that extends continuously across the continental slope over an area of 45,000 km^2, on the much larger Amazon fan a discontinuous BSR has been recognised within a 28,000 km^2 area of the upper slope (Sad et al. 1998; Tanaka et al. 2003; Melo et al. 2008). The area of the Amazon fan BSR coincides with a compressional belt resulting from gravitational collapse of the fan (Fig. 1; Melo et al. 2008), and a number of studies have presented one or more seismic profiles showing the crests of thrust-fold anticlines cross-cut by a BSR of varying amplitude and continuity (Sad et al. 1998; Tanaka et al. 2003; Melo et al. 2008, 2009; Reis et al. 2010; Berryman et al. 2015; Ketzer et al. 2018; Aguiar et al. 2019).

Draft

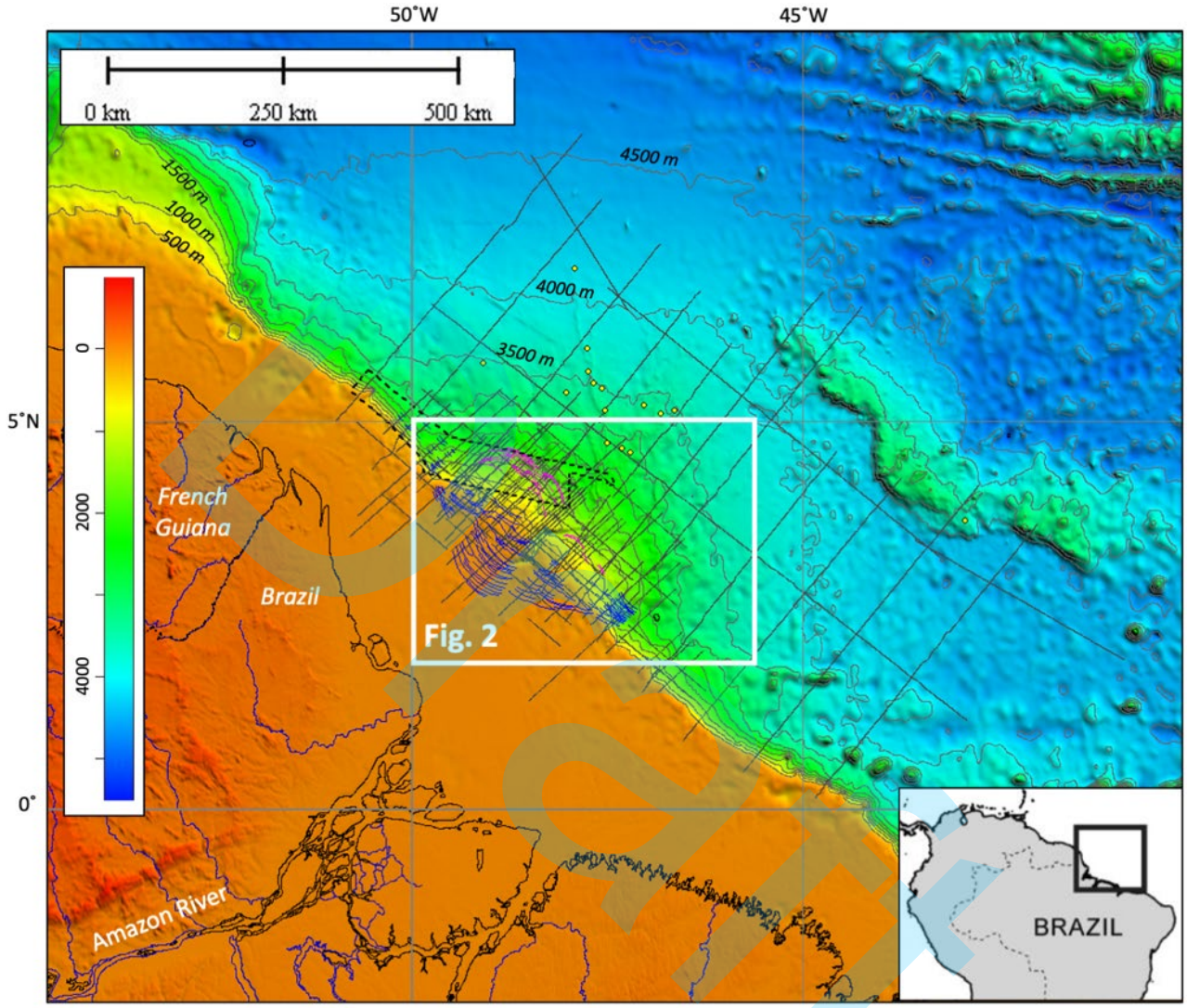

Figure 1 – Location of the Amazon deep-sea fan on the equatorial margin of Brazil (shaded-relief bathymetry from GEBCO 2008), and the available grid of 2D multichannel seismic reflection data (black lines). Arcuate colored lines on the shelf and upper slope correspond to the seafloor traces of paired belts of extensional (blue) and compressional (magenta) faults resulting from gravitational collapse of the fan above deep detachments (from Perovano et al. 2009). Yellow dots denote ODP leg 155 drilling sites, several of which provided indirect indications of the presence of gas hydrates on the mid- to lower slope (Flood et al. 1995, 1997). Dashed box shows the area of multibeam hydroacoustic data presented by Ketzer et al. (2018).

The extent of the Amazon fan BSR was first mapped by Manley and Flood (1988), who used a set of single-channel profiles acquired along the main canyon to trace a BSR across an area of ca. 2500 km^2 above water depths of 1700 m, noting its association with what they referred to as diapir-like structures.

Subsequently, a regional grid of multichannel seismic profiles (Fig. 1) was used to identify multiple BSR patches across the upper slope in water depths of 900-2500 m, each up to tens of kilometres in extent (Tanaka et al. 2003). These authors showed the BSR patches to have no clear orientation but to coincide in part with faults and compressive structures, and also observed small-scale relief of the BSR and of the suprajacent seafloor, together suggested to indicate structurally-controlled seafloor venting of hydrocarbons from deep sources (Tanaka et al. 2003).

Seafloor venting of gas from the compressive belt was confirmed by multibeam imagery acquired in 2016 across part of the upper fan (Fig. 1), which revealed dozens of gas flares rising from low (10-20 m) seafloor mounds, most located along seafloor lineaments identified as faults (Ketzer et al. 2018). The flares lie in water depths of 650-1800 m, within the methane hydrate stability zone and along its upper edge, which is estimated from water column temperatures to lie in depths of 500-670 m (Figs 2, 3; Ketzer et al. 2018, 2019). Gas hydrates cored from two sites on the upper fan (Fig. 3) were shown to contain methane isotopically consistent with biogenic sources (Ketzer et al. 2018). Downslope of the compressive belt, indirect indications of gas hydrate are available from several ODP drill sites on the central to lower Amazon fan (Fig. 1) in the form of low chlorinity pore waters, honeycomb structures and elevated sonic log velocities (Flood et al. 1995, 1997), but no BSRs or venting features have been reported.

The aim of this contribution is to examine the extent and character of the BSR across the upper slope of the Amazon deep-sea fan, based on systematic mapping using a regional grid of 2D and 3D multichannel seismic reflection data (Fig. 1). The results show for the first time that the BSR consists of elongate patches (Figs 2, 3) and provides new information on their relation to subjacent compressional structures as well as to seafloor fluid vents, including venting features newly identified from 3D seismic data (Figs 3-5). Our findings offer insights into the relation of discontinuous BSRs to structurally-controlled fluid flux within collapsing deep-sea depocenters.

Draft

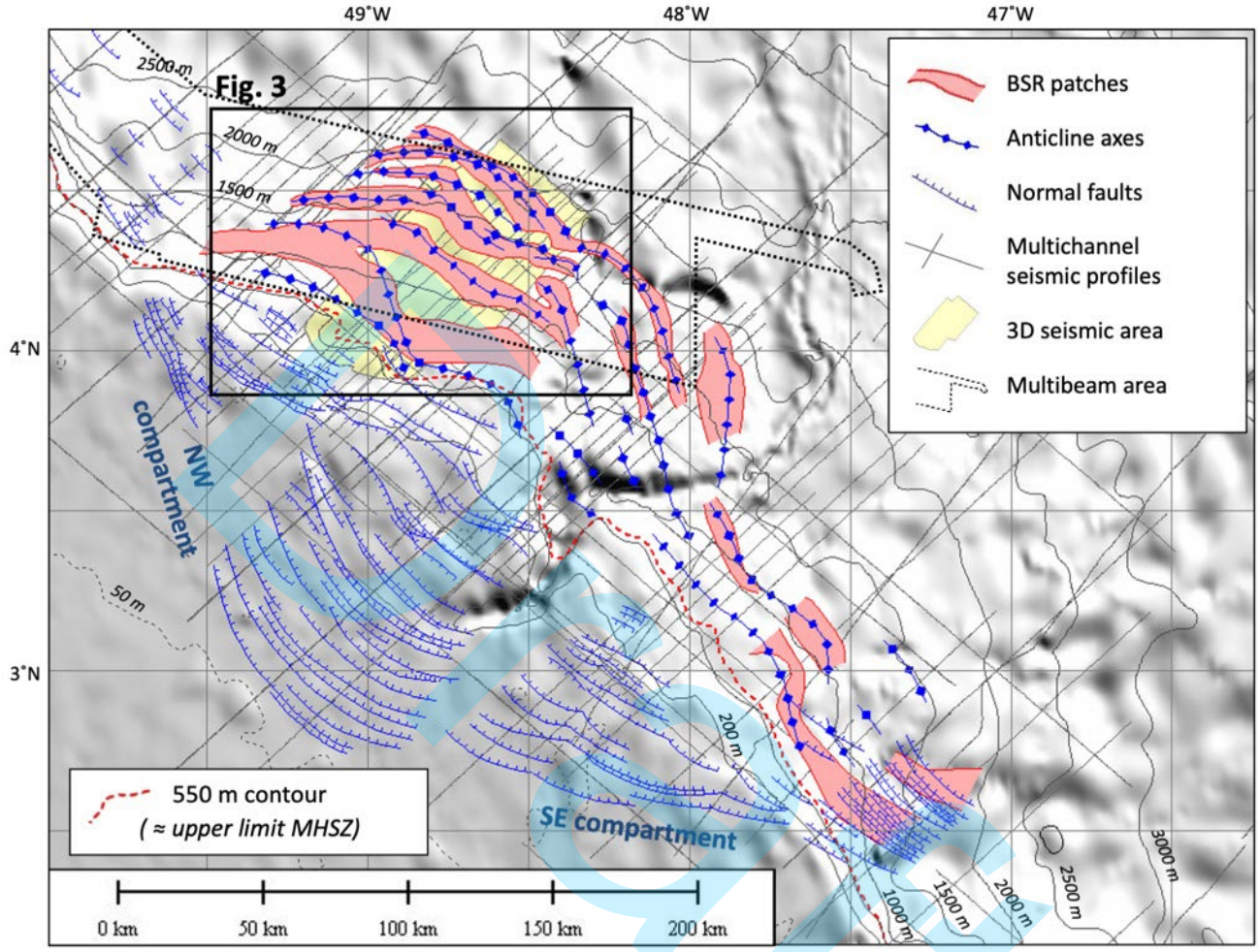

Figure 2 – BSR distribution across the upper Amazon fan (location shown in Fig. 1) as mapped from the regional grid of seismic data, relative to that of structural features mapped by Perovano et al. 2009); the axes of thrust-fold anticlines at seafloor or in the subsurface have been modified for this study. Bathymetric contours derived from GEBCO (2008; the 550 m contour approximates the upper limit of the MHSZ (methane hydrate stability zone), see Ketzer et al. (2019). Area of multibeam data coverage from Ketzer et al. (2018). Data extracts are available from the 3D seismic area (see Fig. 3).

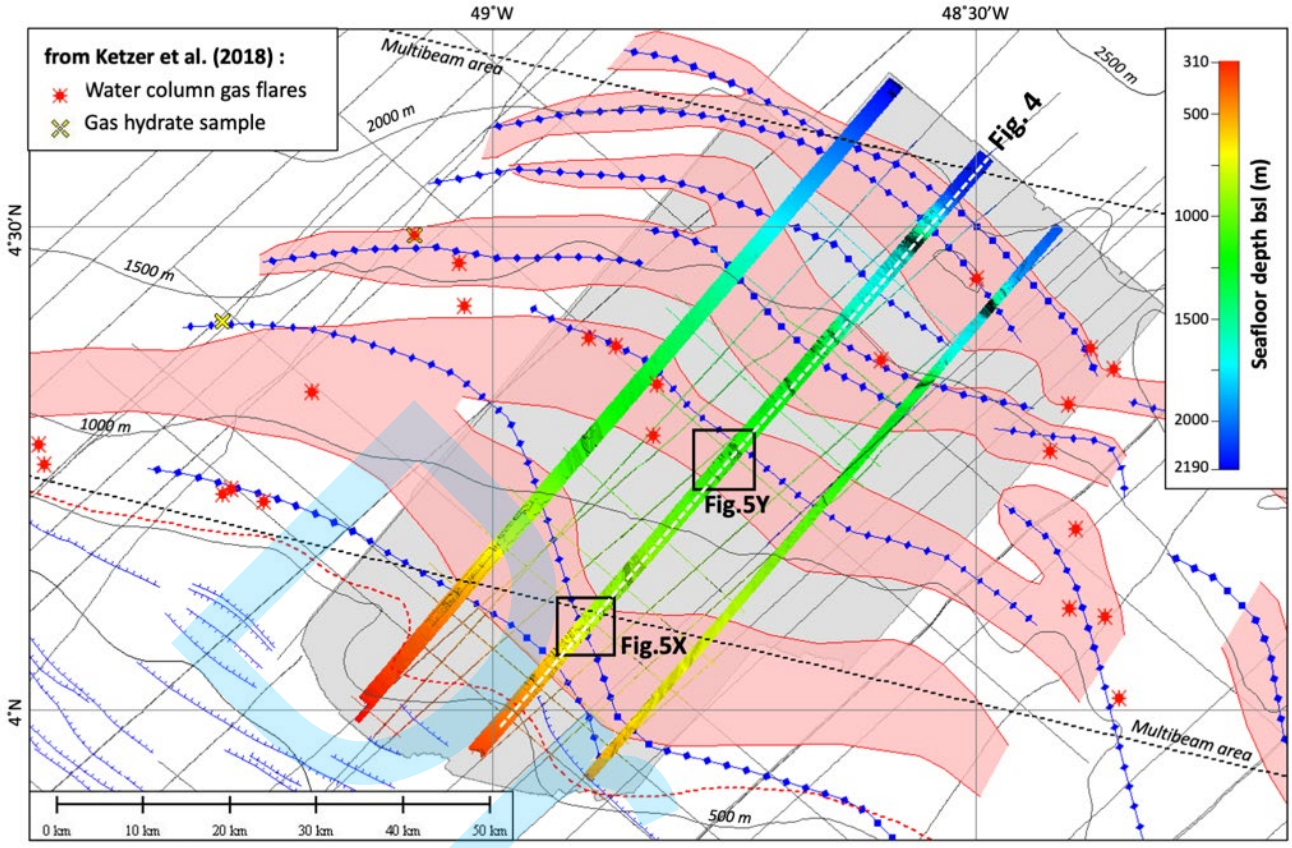

Figure 3 – Detail of BSR distribution in the NW compartment of the Amazon fan (see legend in Fig. 2). Coloured strips show seafloor bathymetry obtained from 3D seismic in-line extracts 1-2 km wide; seafloor depths in metres below seafloor (bsf) based on a velocity of 1.5 km/s. Also shown within the 2016 multibeam survey area (see Fig. 2; Ketzer et al. 2018) are the locations of water column gas flares (red symbols) and of gas hydrates sampled in sediment cores (yellow symbols).

2. Regional Setting

The continental margin of equatorial Brazil dates from the opening of the Central Atlantic in the Early Cretaceous (Matos 2000). During the late Neogene, Andean uplift and associated intra-plate tectonism culminated in the development of a trans-continental Amazon River (Figueiredo et al. 2009; Hoorn et al. 1995, 2010). The Amazon River has among the world's largest discharges of water, sediment and organic matter (Damuth and Kumar 1975; Richey et al. 1980) and culminates in one of the world's largest deep-sea fans, which extends from the mouth of the Amazon River to water depths of at least 4500 m (Fig. 1). Stratigraphic correlations of offshore seismic to well data indicate the Amazon fan to record increased sediment supply from the late Miocene onwards, resulting in the progradation of a

shelf-slope prism up to 10 km thick (Silva et al. 1999; Cobbold et al. 2004; Reis et al., 2010; Hoorn et al. 2017; Cruz et al. 2019).

The growth of the fan has been accompanied by its gravitational collapse above shale detachments at depths of up to 10 km to form paired extensional and compressional belts across the outer shelf and upper slope (Fig. 1; Silva et al. 1999; Perovano et al. 2009; Reis et al. 2010, 2016). The paired structural belts extend NW-SE along 300 km of the shelf and slope above water depths of 2500 m (Fig. 2). They are divided into asymmetric structural compartments, separated by the main Amazon canyon : the NW compartment is >200 km wide and characterized by extensional faults and complex thrust-structures rooted on detachments at depths of up to 10 km, whereas the SE compartment is narrower (<100 km) and contains fewer faults that root on a single deep detachment (Cobbold et al. 2004). In both compartments, thrust-folds are present on the upper slope in water depths greater than about 500 m and include both buried structures as well as, in the NW compartment, seafloor features up to 500 m in relief (Perovano et al. 2009; Reis et al. 2010, 2016).

Tectonic movements within the upper fan compressional belt have been proposed to be responsible for the triggering of slope failures throughout the late Neogene, recorded within the stratigraphic succession of the Amazon fan by stacked megaslides up to hundreds of metres thick that extend up to hundreds of kilometres across the central to lower fan (Reis et al. 2010, 2016). Scientific drilling of four megaslides on the central fan during ODP Leg 155 (Fig. 1) indicated their emplacement from source areas on the upper fan over the last 45 ka during periods of rapidly falling or rising sea level (Flood et al. 1997; Maslin et al. 1998). The results were argued to be consistent with triggering of failure by changes in sedimentation rates and, for two cases of falling sea levels, by associated changes in gas hydrate stability (Maslin et al., 1998).

Draft

3. Data and Methods

The study is based on a regional grid of multichannel seismic (MCS) reflection (MCSR) data acquired for hydrocarbon exploration that includes both 2D profiles and extracts from a 3D seismic volume acquired in 2004 on the upper Amazon fan (Figs 1, 2). The data were acquired over several decades and the quality of imaging varies between individual surveys due to differences in acquisition geometry, frequency content and processing. In general, the MCS data were acquired over recording windows of 6-10 s, and processed using standard sequences of deconvolution, stack and post-stack time migration. Broadband frequency contents <100 Hz correspond to vertical resolution of up to a few tens of metres in the near-surface interval of interest (<1 s below seafloor). All data were visualised and interpreted in a workstation environment.

The spacing of data within the regional grid is higher in the alongslope direction, varying along the upper slope from 5-10 km in the NW to 10-30 km in the SE (Fig. 2). The highest density of data is available from the 3D seismic extracts, which consist of three strips 1-2 km wide and 84-96 km long, covering a total area of 465 km^2 in water depths of 223-2206 m (Fig. 3). The 3D seismic data have an in-line CDP spacing of 6.25 m and a cross-line bin spacing of 12.5 m. These data were used to pick the seafloor reflector along each in-line in order to generate seafloor bathymetric maps (converted from TWT at 1.5 km/s) with a grid resolution of 10 m, and to pick the BSR along selected in-lines to generate depth maps with a grid resolution of 100 m.

4. RESULTS

We first present the seismically-mapped distribution of the BSR, which is seen to consist of a series of elongate patches closely aligned with gravity structures within the upper slope compressional belt (Figs 2, 3). We then consider the character of the BSR patches on seismic profiles and show them to include irregular relief, rising in places towards seafloor (Fig. 4). Finally, we present their relation to seafloor fluid vents, including features newly identified from 3D seismic data (Fig. 5).

Draft

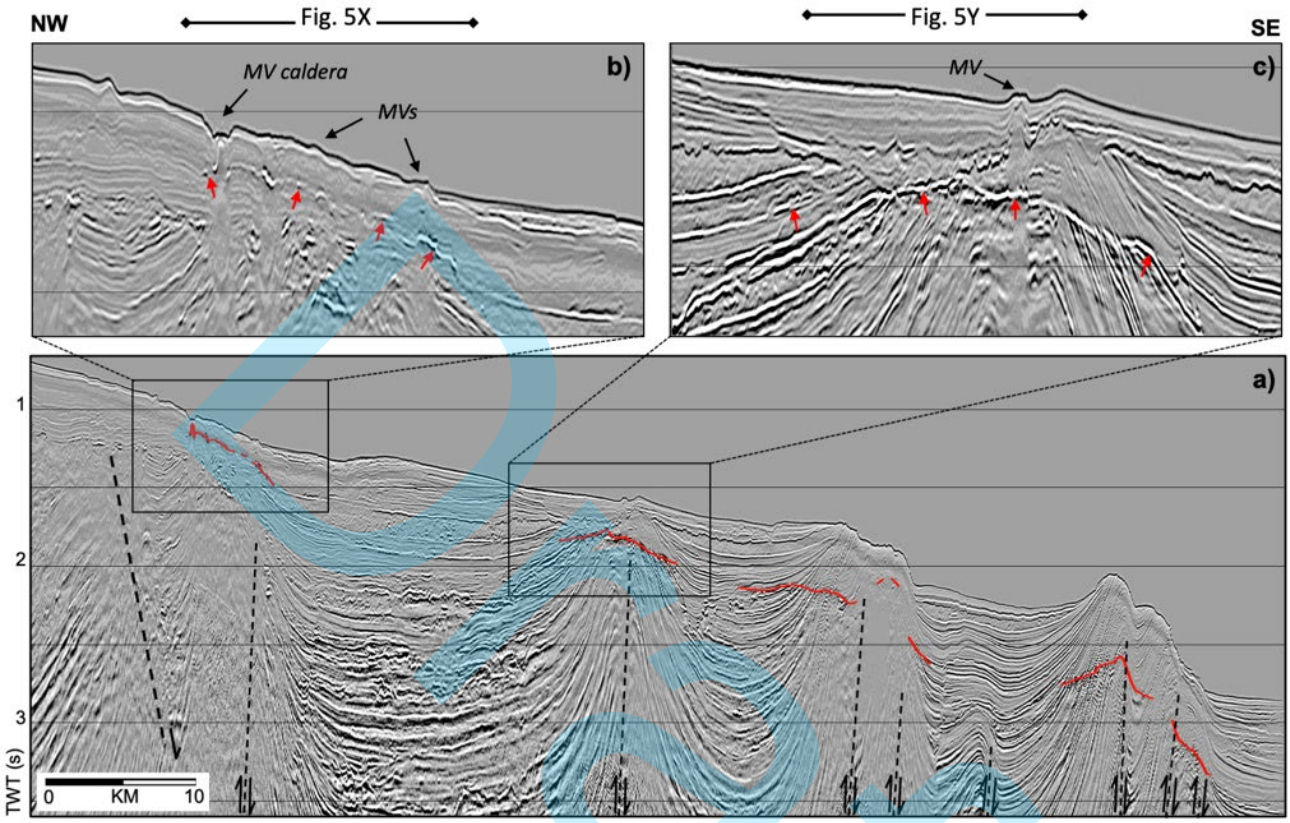

Figure 4 –BSR patches observed in profile along a 3D seismic in-line (location in Fig. 2): a) cross-slope profile showing thrust-fold anticlines associated with four BSR patches (gaps correspond to intervals where the BSR cannot be traced); b, c) details of two BSR patches, each of laterally varying amplitude and continuity, displaying convex cross-sections and irregular small-scale relief beneath features of seafloor venting (see 3D seismic horizon maps in Fig. 4). MV = mud volcanoes.

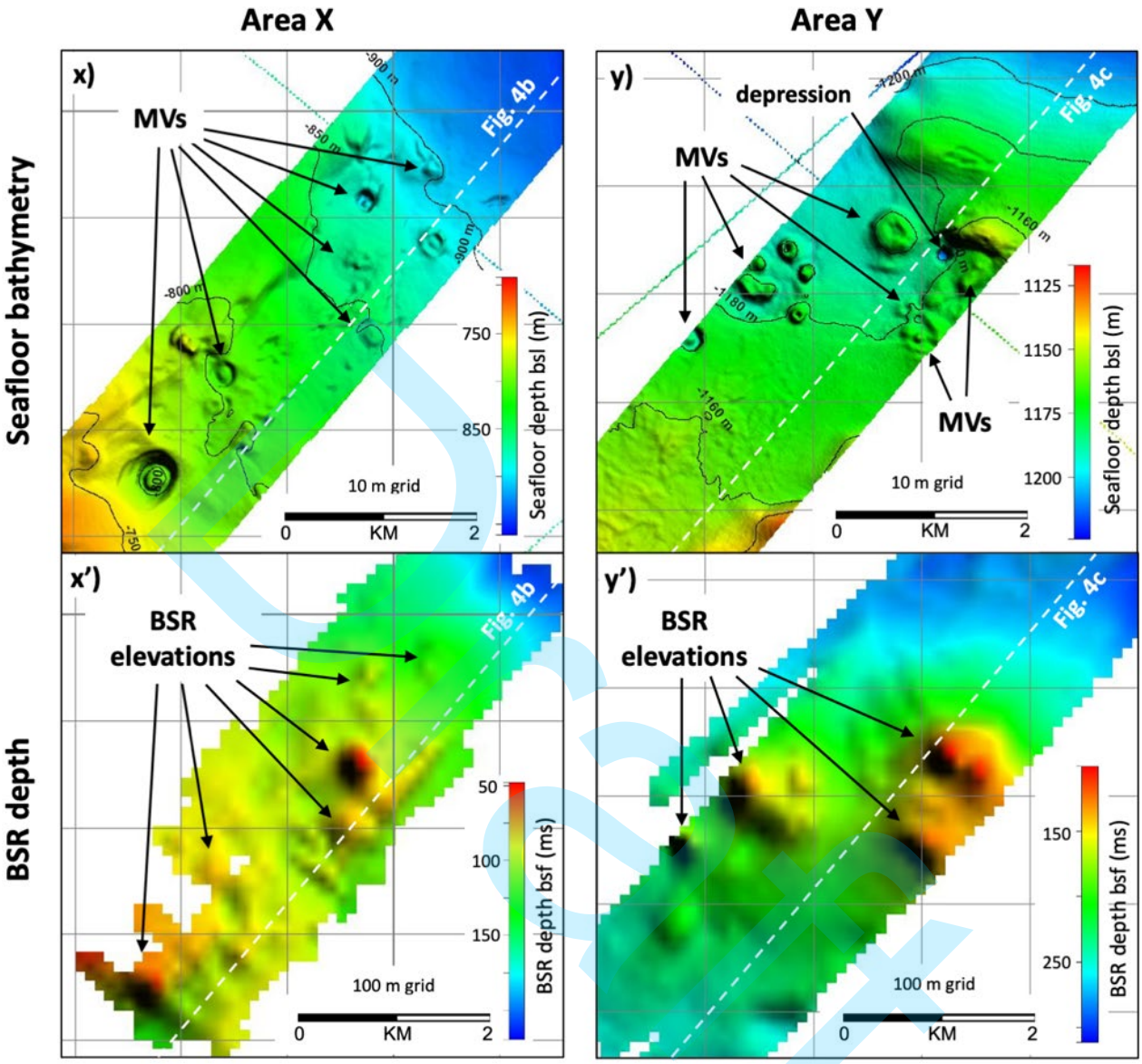

Figure 5 – 3D seismic horizon maps of seafloor bathymetry (top) and BSR relief (bottom) in two areas (locations X and Y shown in Fig. 3; dashed lines correspond to trace of seismic in-line shown in Fig. 4). Seafloor bathymetry has been converted to metres below sea level (bsl) for a water velocity of 1.5 km/s; BSR depths are in milliseconds (ms) two-way travel time below seafloor (bsf). In both areas, the seafloor exhibits mounds and/or depressions interpreted as seafloor fluid vents; note that the subjacent BSR rises towards seafloor beneath some (but not all) fluid vents. MVs = mud volcanoes.

4.1 BSR patches in map view

The BSR extent mapped from the seismic dataset is presented in Fig. 2, together with that of extensional and compressional structures of the NW and SE structural compartments. The axes of thrust-fold anticlines were modified for this study from those mapped by Perovano et al. (2009).

The BSR is seen for the first time to form a series of elongate patches, up to 16 km wide, that extend along 300 km of the upper slope in water depths of 750-2250 m (Fig. 2). The axial continuity of the BSR patches (and of the thrust-fold axes) is less well constrained in the SE compartment due to lower data density. As mapped, the BSR patches cover a total area of 6800 km^2, or less than 25% of the upper slope BSR area indicated in previous studies (Sad et al. 1998; Melo et al. 2008). Consistent with these regional studies, no BSR is recognised in greater water depths across the middle to lower fan.

The elongate BSR patches form an arcuate belt that shows a close spatial relationship to the axes of thrust-fold anticlines, in trend, extent and number (Fig. 2). Each BSR patch coincides along all or part of its length with at least one anticline axis, and the numbers of patches and anticlines both decrease from the NW to SE structural compartments. In the NW compartment, where seismic data density is higher, up to five BSR patches are recognised across the slope in depths of 750-2250 m, in association with seven anticlines; the BSR patches are seen to merge or diverge along their lengths to form an interconnected network, in places following thrust-fold axes and in others crossing from one axis to another (Figs 2, 3). In the SE compartment, two BSR patches in water depths of 750-1250 m coincide with the inner of four anticlines; the BSR patches are of uncertain axial continuity but are tentatively shown to extend downslope beyond the thrust-fold belt into an area of extensional faults in water depths of up to 2000 m (Fig. 2). The two BSR patches are drawn to follow the orientations of these extensional faults, which previous studies have interpreted to be slope-transverse (Tanaka et al. 2003; Perovano et al. 2009). However, low data density in this area makes it difficult to be sure of the orientations of either the faults or the BSR patches, either of which might alternatively be drawn as slope-parallel.

Draft

4.2 BSR patches in profile

On seismic profiles, the BSR is recognised as a negative polarity reflection that cross-cuts dipping stratal reflections at depths below seafloor (bsf) of 80-780 ms (Fig. 4). The BSR varies in amplitude and continuity within the patches, which in places contain short gaps, some coincident with faults within the anticlines (Fig. 4). The BSR fades out laterally at the edges of patches (Fig. 4), the limits of which were generally consistent between adjacent seismic profiles, although variations in extent were noted in places due to differences in source data characteristics or profile orientation (cf. Hillman et al. 2017).

The BSR is mainly observed within or above the crests of thrust-folds and extends to one or both sides of them over distances of a few kilometres, fading out within the more gently dipping strata of intervening ‘piggy-back' basins (Fig. 4). However, in the NW compartment, the innermost BSR patch can in two areas be traced up to 20 km from the nearest thrust-fold axis as a weak reflection that cross-cuts upper slope strata, and extends to within 10 km of the pinch-out of the gas hydrate stability zone (Fig. 3). In addition, in the SE compartment, the two BSR patches are inferred to extend downslope beyond the thrust-fold belt into an area of extensional faults, although low data density makes the orientations of the BSR patches and faults tentative, as noted above (Fig. 2).

In cross-section, many BSR patches exhibit an overall convex form, rising gently towards the seafloor in their central parts, even in the absence of corresponding seafloor relief (Fig. 4a). The BSR in these and other places may also exhibit irregular relief of smaller scale, in which it rises steeply towards the seafloor (Fig. 4b,c), in a manner comparable to what have been referred to elsewhere as ‘pluming BSRs’ (Shedd et al. 2012). Within the 3D seismic dataset, maps of BSR depth in two such locations show the irregular relief to correspond to a series of columnar elevations with diameters of up to 1 km, within which the BSR rises by as much as 200 ms (Fig. 5x’ and 5y’).

Draft

4.3 Seafloor fluid vents

In some areas of irregular BSR relief, bathymetric maps constructed from 3D seismic data (Fig. 3) reveal the seafloor to include semi-circular mounds and depressions, which we interpret as fluid vents, comparable to assemblages of mud volcanoes and pockmarks observed above BSRs on other margins (e.g. Benjamin and Huuse 2017; Serié et al. 2017). Two such areas of irregular BSR relief along Fig. 4 are mapped and compared to seafloor relief in Fig. 5.

Figure 5x shows an area in water depths of 750-950 m, where the seafloor includes a variety of semi-circular features, including mounds, mounds that lie within depressions, and depressions, up to 0.5 km wide and up to 30 m in relief. Figure 5y shows an area in water depths of 1120-1220 m, where the seafloor includes sub-circular mounds up 0.5 km wide and 20 m high, some of which occupy depressions, as well a depression up to 30 m between mounds. In both areas, some of the mounds include distinctive crater-like depressions at their summits (Fig. 5x,y). Seismic profiles across the mounds and depressions show them to form the top of unstratified columns that extend downward over 1 km into the thrust-folds (e.g. Fig. 4b,c).

The mounds are consistent in their morphology and subsurface character with extrusive features, i.e. relatively small mud volcanoes recording seafloor sediment extrusion from subsurface plumbing networks that extend to depths of kilometres (Kopf 2002; Dimitrov 2002; Deville et al. 2010; Benjamin and Huuse 2017). Some of the mud volcanoes contain calderas at their summits, while others occupy larger caldera-like depressions; caldera formation is consistent with localised subsidence due to loss of fluid pressures and/or extrusion of sediment from shallow mud chambers within or beneath the mounds (Henry et al. 1996; Planke et al. 2003). Isolated depressions observed in both areas (Fig. 5x,y) could also correspond to subsidence depressions, or alternatively to large pockmarks, which may occur peripheral to mud volcanoes (e.g. Dimitrov and Woodside 2003; Samoza et al. 2012; Benjamin and Huuse 2017).

Draft

In both areas, maps of BSR depth show it to include irregular relief, including columnar elevations up to 1 km wide that rise towards seafloor (Fig. 5x',y'). These BSR elevations all coincide with seafloor mounds and/or depressions (cf. Fig. 5x,y). Interestingly, however, some seafloor features do not coincide with BSR elevations (compare top and bottom panels of Fig. 5).

5. DISCUSSION

The results presented above provide a new picture of the extent and character of the discontinuous gas hydrate BSR on the upper Amazon fan and its relationship to structures within the compressional belt. Previous studies have noted the association of the BSR with thrust-fold anticlines, and with possible evidence of seafloor gas venting (Tanaka et al. 2003; Melo et al. 2008; Reis et al. 2010; Ketzer et al. 2018). Our results provide the first clear demonstration of a strong spatial correlation between elongate BSR patches and the crests of thrust-folds within the arcuate structural belt (Figs 2-4), and provide strong evidence that both the lateral discontinuity and irregular relief of the BSR patches is related to upward fluid migration through the thrust-folds (Figs 4, 5).

5.1 BSR patches formed by structurally-controlled fluid flow

BSRs are discontinuous at varying scales, and the term 'patch' has also been applied to features having short gaps of <1 km, which may reflect lateral heterogeneities in lithology and/or in the supply of gas (Shedd et al. 2012; Hillman et al. 2017). The elongate BSR patches on the upper Amazon fan provide a distinctive example of BSR discontinuity on a larger scale (10^1-10^2 km), clearly linked in extent and trend to subjacent thrust-folds (Figs. 2, 3). The BSR patches on the Amazon fan are comparable to those observed on the deep-water Niger delta, which also coincide with the crests of shale anticlines forming the tops of deeply-rooted thrust-folds (Hovland et al. 1997; Cunningham and Lindholm 2000; Sultan et al. 2011). In places on the Niger delta, elongate BSR patches are associated with seismically-interpreted features of fluid venting to seafloor, which together with the BSR are proposed to record the

upward migration of fluids containing hydrocarbon gases by a combination of focused and diffuse flow (Hovland et al. 1997). Although not mapped or described as patches, BSRs that are laterally discontinuous on a kilometric scale are also recognised at the crests of anticlines in the NW Borneo thrust-fold belt and linked to upward fluid migration through the structures (Laird and Morley 2011; Morley et al. 2014; McGiveron and and Jong 2018). In general, these studies show that thrust-fold belts are associated with the migration from depth of overpressured fluids, via structural and stratal pathways that promote a confluence of fluids at the crests of anticlines, and their leakage to surface through faults and hydrofractures that develop at shallow (<1 km) depths (Morley et al. 2014).

In the Amazon fan, fluid overpressures to drive gravitational collapse have been proposed to arise from hydrocarbon generation at thermogenic depths beneath the fan (Cobbold et al. 2004). However, basin modelling suggests that thermogenic fluids remained trapped in strata beneath the fan, within which structurally-compartmentalised overpressures arise due to a combination of disequilibrium compaction and clay mineral transitions (Gonçalves Souza et al. 2020). The presence of seafloor mud volcanoes within areas of BSR occurrence (Figs 4, 5) provides clear evidence that in places within the fan, overpressured fluids are rising from depth by focused flow through the thrust-folds. However, the mud volcanoes form point-source features within BSR patches that extend across the crests of the anticlines over distances of up to 16 km and along their axes for distances >100 km (Figs 2, 3). The overall continuity of the BSR patches across such distances can be explained in terms of broad zones of near-surface leakage at the crests of the anticlines, in which gas-rich fluids are released by diffuse flow through systems of seismically observable faults and sub-seismic fractures (cf. Hovland et al. 1997; Morley et al. 2014). It is interesting to note that in places, seismically-observed faults coincide with short gaps in the BSR patches (Fig. 4), consistent with a structural compartmentalisation of fluid flow and near-surface leakage within the anticlines. In an analogous manner, the lateral fading out of the BSR patches could be understood in terms of a reduced supply of gas-rich fluids away from the thrust-folds, until it becomes insufficient to give rise to a BSR (cf. Haacke et al. 2007).

Draft

5.2 BSR relief controlled by heat flux

Several factors may influence the depth of a BSR, including variations in the velocity and thermal transmissivity of near-surface sediments, topographic effects on conductive heat flow, heat transport by fluid advection, and the composition of pore fluids and gas (e.g. Riedel et al. 2010). Within thrust-folds, the presence of older strata with higher velocities and transmissivities might cause the BSR to rise; at the same time, where thrust-folds have seafloor expression, heat dispersion from positive relief might cause the BSR to deepen. However, the association of small-scale BSR elevations with seafloor fluid vents (Fig. 5) strongly points to a dominant influence of fluid advection and heat transport on BSR depth (e.g. Shedd et al. 2012; Serié et al. 2017). The rise of warm fluids may also involve changes in fluid and gas compositions, such that the advection of saline pore fluids or of higher hydrocarbons could significantly decrease or increase gas hydrate stability, respectively (Sloan 2003). However, there is no evidence for evaporitic deposits in or beneath the Amazon fan (Cruz et al. 2019), and while basin modelling confirms the potential for thermogenic hydrocarbon generation and migration beneath the basal detachment of the collapse system (Souza et al. 2020), gas hydrates cored at two venting sites on the upper fan (Fig. 3) are composed predominantly of microbial methane (Ketzer et al. 2018).

The convex and/or irregular relief observed within individual BSR patches (Figs 4, 5) can thus be interpreted in terms of spatial variability in the upward flux of warm fluids, with highest (focused) flux through the conduits feeding mud volcanoes. A varying fluid flux also implies variations in the supply of gas, and it is interesting to note that in places, changes in BSR depth correlate with variations in amplitude and continuity, including short gaps (Fig. 4). Studies in areas with drilling data provide evidence of a clear correlation between BSR elevations, heat and fluid flux and gas hydrate concentrations (Hornbach et al. 2012). The morphology of the BSR patches thus suggests that the Amazon fan gas hydrate province may include rich concentrations of gas hydrates.

Draft

The BSR is observed to rise beneath some seafloor fluid vents, but not all of them (Fig. 5). Assuming BSR depth is controlled by heat transport, this could indicate that some seafloor features are associated with on-going or recent fluid advection, while others are inactive or have not recently been active. This would be consistent with the behaviour of mud volcanoes and pockmarks, both of which are inherently episodic in their emissive activity (Kopf 2002; Planke et al. 2003; Deville et al. 2010). The size range of the mud volcanoes observed on 3D seismic data (Fig. 4) encompasses that of seafloor mounds previously observed on multbeam data acquired in 2016 across the upper Amazon fan, from some of which gas flares were observed rising into the water column at 23 locations (red stars in Fig. 3; Ketzer et al. 2018). Comparison with the BSR distribution shows that most of the degassing mounds lie above thrust-fold anticlines and within BSR patches (Fig. 3), which were thus venting gas through the seafloor at multiple sites in 2016. Interestingly, however, none of the features observed on 3D seismic data were venting gas to the water column (Fig. 3).

CONCLUSIONS

Systematic mapping of a BSR across the upper Amazon fan using a regional grid of 2D and 3D seismic data shows for the first time that it consist of elongate patches, up to 16 km wide, that show a strong spatial correspondence with the arcuate crests of thrust-fold anticlines within an upper slope compressional belt. In cross-section the BSR patches in places exhibit convex forms and/or irregular relief, while in plan 3D seismic horizon maps reveal columnar BSR elevations beneath seafloor fluid escape features (small mud volcanoes, possible pockmarks). The BSR patches are interpreted to provide evidence of the rise of warm gas-rich fluids through the thrust-folds and their leakage into and through the gas hydrate stability zone via a near-surface system of faults, hydrofractures, and fluid vents. This process may have resulted in the formation of concentrated gas hydrate deposits.

Draft

ACKNOWLEDGEMENTS

The seismic reflection dataset was obtained from ANP. The senior author's collaboration with Brazilian and French colleagues was made possible by funding from the European Union's Horizon 2020 research and innovation program under Marie Skłodowska-Curie grant agreement No. 656821 (project SEAGAS, 2016-2020), and by a visiting fellowship at the Universidade Federal Fluminense (2018-2019) from the Brazilian agency CAPES (Coordenação de Aperfeiçoamento de Pessoal de Nível Superior, Edital IODP 38/2014). We also thank Seismic Micro-Technology Inc. for the use of educational licenses of the software Kingdom Suite®. Cleverson Guizan Silva and Antonio Tadeu dos Reis received research grants No. 313086/2017-6 and No. 309297/2018-4 from the Brazilian National Research Council (CNPq). This is a contribution of the research group GEOMARGEM: Geology and Oceanography of Passive Margins (http:// www.geomargem.org).

REFERENCES

Aguiar L.F., Freire A.F.M., Santos L.A., Dominguez A.C.F., Neves E.H.P., Silva C.G., Santos M.A.C. (2019). Analysis of seismic attributes to recognize bottom simulating reflectors in the Foz do Amazonas Basin, northern Brazil. *Brazilian Journal of Geophysics*, 37(1), 43-53.

Archer D., Buffett B., Brovkin V. (2009). Ocean methane hydrates as a slow tipping point in the global carbon cycle. *Proceedings of the National Academy of Sciences U.S.A.*, 106(49), 20,596–20,601, doi:10.1073/pnas.0800885105.

Benjamin U.K., Huuse M. (2017). Seafloor and buried mounds on the western slope of the Niger Delta. *Marine and Petroleum Geology*, 83, 158-173, doi:10.1016/j.marpetgeo.2017.02.023.

Berryman J., Kearns H., Rodriguez K. (2015). Foz do Amazonas Basin - A case for oil generation from geothermal gradient modelling. *First Break*, 33, 91–95.

Boswell R., Collett T.S. (2011). Current perspectives on gas hydrate resources. *Energy & Environmental Science*, 4(4), 1206–1215, doi:10.1039/ c0ee00203h.

Cobbold P.R., Mourgues R., Boyd K. (2004). Mechanism of thin-skinned detachment in the Amazon Fan: assessing the importance of fluid overpressure and hydrocarbon generation. *Marine and Petroleum Geology* 21, 1013–1025.

Draft

Cruz A.M., Reis A.T., Suc J., Silva C.G., Praeg D., Granjeon D., Rabineau M., Popescu S., Gorini C. (2019). Neogene evolution and demise of the Amapá carbonate platform, Amazon Continental Margin, Brazil. *Marine and Petroleum Geology*, 105, 185-203, doi:10.1016/j.marpetgeo.2019.04.009.

Cunningham R., Lindholm R.M. (2000). Seismic evidence for widespread gas hydrate formation, offshore west Africa. In: Mello M.R. and Katz B.J. (Editors), *Petroleum Systems of South Atlantic Margins*; American Association of Petroleum Geologists Memoir 73, 93-105, doi:10.1306/M73705C8.

Damuth J.E., Kumar N. (1975). Amazon Cone: morphology, sediments, age, and growth pattern. *Geological Society of America Bulletin*, 86, 863-878.

Deville E., Guerlais S.-H., Lallemant S., Schneider F. (2010). Fluid dynamics and subsurface sediment mobilization processes: an overview from Southeast Caribbean. *Basin Research*, 22, 361–379, doi: 10.1111/j.1365-2117.2010.00474.x.

Dimitrov L.I. (2002). Mud volcanoes – the most important pathway for degassing deeply buried sediments. *Earth-Science Reviews*, 59, 49–76.

Dimitrov L., Woodside J. (2003). Deep sea pockmark environments in the eastern Mediterranean. *Marine Geology*, 195, 263–276.

Figueiredo J., Hoorn C., van der Ven P., Soares E. (2009). Late Miocene onset of the Amazon River and the Amazon deep-sea fan: evidence from the Foz do Amazonas Basin. *Geology*, 37:619–622, doi:10.1130/G25567A.1.

Flood R.D., Piper D.J.W., Klaus A., et al. (1995). *Proceedings of the Ocean Drilling Program, Volume 155, Initial Reports, Amazon Fan*. College Station, Texas, USA (Ocean Drilling Program), 1233 pp., doi:10.2973/odp.proc.ir.155.1995.

Flood R.D., Piper D.J.W., Klaus A., Peterson L.C. (1997), *Proceedings of the Ocean Drilling Program, Volume 155, Scientific Results, Amazon Fan.* College Station, Texas, USA (Ocean Drilling Program), 695 pp, doi:10.2973/odp.proc.sr.155.1997.

Fontana R.L., Mussumeci A. (1994). Hydrates offshore Brazil. *Annals of the New York Academy of Sciences*, 715, 106–113.

GEBCO (2008). *General Bathymetric Chart of the Oceans*, GEBCO_08 30 Arc-Second Grid, version 20091120, http://www.gebco.net.

Gonçalves Souza J.M., Cubas N., Rabe C., Letouzey J., Divies R., Praeg D., Granjeon D., Cruz A.M., Silva C.G., dos Reis A.T., Gorini C. (2020). Controls on overpressure evolution during the gravitational collapse

Draft

of the Amazon deep-sea fan. *Marine and Petroleum Geology*, 121, 104576, doi:10.1016/j.marpetgeo.2020.104576.

Haacke R.R., Westbrook G.K., Hyndman R.D. (2007). Gas hydrate, fluid flow and free-gas: Formation of the bottom-simulating reflector. *Earth and Planetary Science Letters*, 261, 407–420, doi:10.1016/j.epsl.2007.07.008).

Henry P., Le Pichon X., Lallemant S., Lance S., Martin J., Foucher J.P., Fiala-Médioni A., Rostek F., Guilhaumou N., Pranal V., Castrec M. (1996). Fluid flow in and around a mud volcano field seaward of the Barbados accretionary wedge: results from Manon cruise. *Journal of Geophysical Research*, 101 (B9), 20,297–20,323.

Hillman J.I.T., Cook A.E., Sawyer D.E., Küçük H.M., Goldberg D.S. (2017). The character and amplitude of 'discontinuous' bottom-simulating reflections in marine seismic data. *Earth and Planetary Science Letters,* 459, 157-169, doi:10.1016/j.epsl.2016.10.058.

Holbrook, W.S., Hoskins, H., Wood, W.T., Stephen, R.A., Lizarralde, D. (1996). Methane hydrate and free gas on the Blake Ridge from vertical seismic profiling. *Science*, 80(273), 1840–1843.

Hoorn C., Guerrero J., Sarmiento G.A., Lorente M.A. (1995). Andean tectonics as a cause for changing drainage patterns in Miocene northern South America. *Geology*, 23, 237–240, doi:10.1130/0091-7613(1995)023b0237:ATAACFN2.3.CO;2.

Hoorn C., Wesselingh F.P., ter Steege H., Bermúdez M.A., Mora A., Sevink J., Sanmartín I., Sanchez-Meseguer A., Anderson C.L., Figueiredo J.P., Jaramillo C., Riff D.D., Negri F.R., Hooghiemstra H., Lundberg J., Stadler T., Särkinen T., Antonelli A. (2010). Amazonia through time: Andean uplift, climate change, landscape evolution and biodiversity. *Science*, 330, 927–931, doi:10.1126/science.1194585.

Hoorn C., Bogotá-A G.R., Romero-Baez M., Lammertsma E.I., Flantua S.G.A., Dantas E.L., Dino R., do Carmo D.A., Chemale F. (2017). The Amazon at sea: onset and stages of the Amazon River from a marine record, with special reference to Neogene plant turnover in the drainage basin. *Global and Planetary Change*, 153, 51–65, doi:10.1016/j.gloplacha.2017.02.005.

Hornbach M.J., Bangs N.L., Berndt C. (2012). Detecting hydrate and fluid flow from bottom simulating reflector depth anomalies. *Geology*, 40(3), 227-230.

Hovland M., Gallagher W., Clennell M.B., Lekvam K. (1997). Gas hydrate and free gas volumes in marine sediments: Example from the Niger Delta. *Marine and Petroleum Geology*, 14(3), 245-255.

Draft

Ketzer J.M., Augustin A., Rodrigues L.F., Oliveira R., Praeg D., Pivel M., Reis T., Silva C., Leonel B. (2018). Gas seeps and gas hydrates in the Amazon deep-sea fan. *Geo-Marine Letters*, 38(5), 429-438, doi:10.1007/s00367-018-0546-6.

Ketzer J.M., Praeg D., Pivel M.A.G., Augustin A.H., Rodrigues L.F., Viana A.R., Cupertino J.A. (2019). Gas seeps at the edge of the gas hydrate stability zone on Brazil's continental margin. *Geosciences*, 9, 193, doi:10.3390/geosciences9050193.

Kopf A. (2002). Significance of mud volcanism. *Reviews of Geophysics*, 40 (2), 1–51.

Laird A.P., Morley C.K. (2011). Development of gas hydrates in a deep-water anticline based on attribute analysis from three-dimensional seismic data. *Geosphere*, 7, 1-20.

Majumdar U., Cook A.E., Shedd W., Frye M. (2016). The connection between natural gas hydrate and bottom-simulating reflectors. *Geophysical Research Letters*, 43, 7044–7051, doi:10.1002/2016GL069443.

Manley P.L., Flood R.D. (1988). Cyclic sediment deposition within the Amazon deep-sea fan. *American Association of Petroleum Geologists Bulletin*, 72, 912–925.

Maslin M.A., Mikkelsen N., Vilela C., Haq B. (1998). Sea level controlled catastrophic sediment failures of the Amazon Fan. *Geology*, 26, 1107–1110.

Maslin M., Owen M., Betts R., Day S., Dunkley Jones T., Ridgwell A. (2010). Gas hydrates: Past and future geohazard? *Philosophical Transactions of the Royal Society A, Mathematical, Physical and Engineering Sciences*, 368(1919), 2369–2393, doi:10.1098/rsta.2010.0065.

Matos R.M.D. (2000). Tectonic evolution of the equatorial South Atlantic. In: Mohriak W.U. and Talwani M. (Editors), *Atlantic Rifts and Continental Margins*; AGU Geophysical Monograph Series 115, 331-354.

McGiveron S., Jong J. (2018). Complex geothermal gradients and their implications, deepwater Sabah, Malaysia. *Bulletin of the Geological Society of Malaysia*, 66, 15-22.

Melo F.F., Silva C.G., dos Reis A.T. (2008). Hidratos de gás no leque submarino do Amazonas: ocorrência e formação. III Simpósio Brasileiro de SBGf, Sociedade Brasileira de Geofísica, Belém, PA, Brasil; Expanded Abstracts, 5 pp.

Melo F.F., Silva C.G., dos Reis A.T., Araújo J.E.F. (2009). Transporte de massa e hidratos de gás no leque submarino do Amazonas. 11th International Congress of the Brazilian Geophysical Society, Salvador, BA, Brasil; *Proceedings*, 5 pp., doi:10.3997/2214-4609-pdb.195.2095_evt_6year_2009.

Morley C.K., Warren J., Tingay M., Boonyasaknanon P., Julapour A. (2014). Comparison of modern fluid distribution, pressure and flow in sediments associated with anticlines growing in deepwater (Brunei) and

continental environments (Iran). *Marine and Petroleum Geology*, 51, 210-229, doi:10.1016/j.marpetgeo.2013.11.011.

Perovano R., dos Reis A.T., Silva C.G., Vendeville B., Gorini C., Oliveira V., Araújo E.F.S. (2009). O processo de colapso gravitacional da seção marinha da Bacia da Foz do Amazonas – margem equatorial brasileira. *Revista Brasileira de Geofísica*, 27(3), 459-484.

Planke S., Svensen H., Hovland M., Banks D.A., Jamtveit B. (2003). Mud and fluid migration in active mud volcanoes in Azerbaijan. *Geo-Marine Letters*, 23, 258–268.

Reis A.T., Perovano R., Silva C.G., Vendeville B.C., Araújo E., Gorini C., Oliveira V. (2010). Two-scale gravitational collapse in the Amazon Fan: a coupled system of gravity tectonics and mass-transport processes. *Journal of the Geological Society, London*, 167, 593–604, doi:10.1144/0016- 76492009-035.

Reis A.T., Araújo E., Silva C.G., Cruz A.M., Gorini C., Droz L., Migeon S., Perovano R., King I., Bache F. (2016). Effects of a regional décollement level for gravity tectonics on late Neogene to recent large-scale slope instabilities in the Foz do Amazonas Basin, Brazil. *Marine and Petroleum Geology*, 75, 29–52, doi:10.1016/j. marpetgeo.2016.04.011.

Richey J.E., Brook J.T., Naiman R.J., Wissmar R.C., Stallard R.F. (1980). Organic carbon: oxidation and transport in the Amazon River. *Science*, 207:1348–1351.

Riedel M., Tréhu A.M., Spence G.D. (2010). Characterizing the thermal regime of cold vents at the northern Cascadia margin from bottom-simulating reflector distributions, heat-probe measurements and borehole temperature data. *Marine Geophysical Research*, 31, 1–16.

Sad A.R.E., Silveira D.P., Silva S.R.P., Maciel R.R., Machado, M.A.P. (1998). Marine gas hydrates along the Brazilian margin. *AAPG International Conference, Rio de Janeiro, Extended Abstracts*, 146–147.

Serié, C., Huuse, M., Schødt, N.H., Brooks, J.M., Williams, A. (2017). Subsurface fluid flow in the deep-water Kwanza Basin, offshore Angola. *Basin Research*, 29, 149–179, doi:10.1111/bre.12169.

Shedd W., Boswell R., Frye M., Godfriaux P., Kramer K. (2012). Occurrence and nature of “bottom simulating reflectors” the Northern Gulf of Mexico. *Marine and Petroleum Geology*, 34, 31–40.

Shipley T.H., Houston M.H., Buffler R.T., Shaub F.J., McMillen K.J., Ladd J.W., Worzel J.L. (1979). Seismic evidence for widespread possible gas hydrate horizons on continental slopes and rises. *American Association of Petroleum Geologists Bulletin*, 63, 2204–2213.

Silva S.R.P., Maciel R.R., Severino M.C.G. (1999). Cenozoic tectonics of Amazon Mouth Basin. *Geo-Marine Letters*, 18, 256–262, doi:10.1007/s003670050077.

Draft

Sloan E.D., Jr (2003) Fundamental principles and applications of natural gas hydrates. *Nature*, 426, 353-359.

Somoza L., Medialdea T., León R., Ercilla G., Vázquez J.T., Farran M.-L., Hernández-Molina J., González J., Juan M., Fernández-Puga M.C. (2012). Structure of mud volcano systems and pockmarks in the region of the Ceuta Contourite Depositional System (Western Alborán Sea). *Marine Geology*,

332–334, 4-26.

Sultan N., Riboulot V., Ker S., Marsset B., Geli L., Tary J.B., Klingelhoefer F., Voisset M., Lanfumey V., Colliat J.L., Adamy J., Grimaud S. (2011). Dynamics of fault-fluid-hydrate systems around a shale-cored anticline in deepwater Nigeria. Journal of Geophysical Research, 116, B12110, doi:10.1029/2011JB008218.

Tanaka M.D., Silva C.G., Clennell M.B. (2003). Gas hydrates on the Amazon Submarine Fan, Foz do Amazonas Basin, Brazil. AAPG Annual Meeting, 2003, Salt Lake City, Utah, USA; *AAPG Search and Discovery Article #90013, available on :* http://www.searchanddiscovery.com/pdfz/abstracts/pdf/2003/annual/extend/ndx_78250.PDF.html.

Praeg D.: interpreted the seismic data, prepared the figures, wrote and revised the manuscript;
Silva C.G.: compiled the seismic data, collaborated in its interpretation, arranged facilities and funding to make the study possible;
dos Reis A.T.: collaborated in data interpretation, revised the manuscript, facilitated its submission;
Cruz A.: collaborated in interpretation of the seismic data;
Ketzer J.M.: collaborated in interpretation of fluid flow, revised the manuscript;
Migeon S.: collaborated in interpretations of fluid flow, revised the manuscript;
Gorini C.: regional knowledge of stratigraphy.

Draft